ACS Sustainable Chemistry & Engineering

Research Article

pubs.acs.org/journal/ascecg

A High-Performance Hierarchical Graphene@Polyaniline@Graphene Sandwich Containing Hollow Structures for Supercapacitor Electrodes

Xianbin Liu, Na Wen, Xiaoli Wang, and Yuying Zheng*

College of Materials Science and Engineering, Fuzhou University, 2 Xueyuan Road, Fuzhou 350116, China

Supporting Information

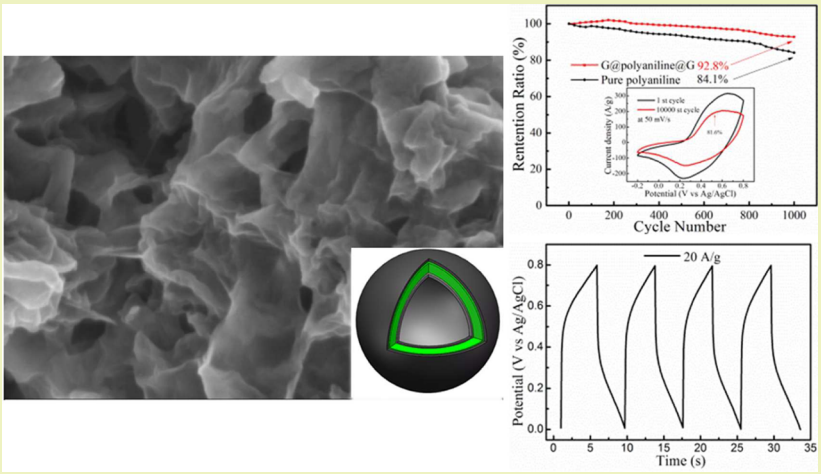

ABSTRACT: An effective design and fabrication of a more steady structure for high-performance electrodes applications still remains a challenge. Herein, we have designed and fabricated a hierarchical heterostructure of a graphene@polyaniline@graphene sandwich consisting of hollow polyaniline spheres as the sandwich layer and graphene both as an internal skeleton shell and a cladding layer. The special sandwich configuration not only enlarged the specific surface area but also improved the electrical conductibility. Most importantly, the graphene double shells could prevent the structural breakdown (swelling or shrinkage) of polyaniline. Therefore, as a supercapacitor electrode, the hybrid exhibited excellent performance with a specific capacitance of 682.75 F g^{-1} at 0.5 A g^{-1} and a remarkable cycling stability with capacitance retentions of 92.8% after 1000 cycles and even 87.6% after 10,000 cycles, which were better than those of pure polyaniline. In addition, the specific capacitance could reach 217.11 F g^{-1} at a high current density of 20 A g^{-1}. Thus, it could be considered as a perspective electrode for the next generation of high-performance supercapacitors.

KEYWORDS: *Polyaniline, Sandwich, Hollow structure, Cycling stability, Supercapacitors*

INTRODUCTION

With the dramatic growth of portable and smart electric production, there is an urgent demand to develop new sustainable and reliable energy storage and supply devices.[1−3] Supercapacitors, also known as electrochemical capacitors, have been considered as next generation power devices owing to their significant advantages including their high power density, fast charge−discharge time, and long life cycle.[4−7] Generally, supercapacitors are classified into two types based on their charge storage mechanisms: electrical double layer capacitors (EDLCs) and pseudocapacitors.[8] The capacitance of EDLCs is generated by charge adsorption at the electrode interface of the active materials such as carbon materials,[9] while the capacitance of pseudocapacitors is generated by a fast and reversible redox or faradic transformation of capacitive materials such as metal oxides and conductive polymers. In comparison, the capacitance values of pseudocapacitors are higher than those of EDLCs, which are limited by microstructures. However, pseudocapacitive materials often exhibit low electrical conductibility and poor stability during the charge−discharge process.[10] Therefore, it is extremely significant to integrate the benefits of the EDLCs and pseudocapacitive materials.

Among the pseudocapacitive materials, polyaniline (PANI) is one of the most extensively investigated materials due to its ease of synthesis, good environmental stability, high electrical conductibility, and great capacitance for energy storage.[8,11−13] In order to improve its performance, nanostructured PANI with various morphologies such as nanowires,[14,15] nanorods,[13,16,17]

Received: November 6, 2014
Revised: January 6, 2015
Published: February 4, 2015

DOI: 10.1021/sc5006999
ACS Sustainable Chem. Eng. 2015, 3, 475−482

and nanofibers[18,19] have been fabricated using different chemical methods. However, PANI experiences structural change during the charge−discharge process, and as a result, the capacitance decays rapidly. Many studies have concentrated on chemical grafting[20−22] or physical coating[23,24] to improve its stability. Graphene, a two-dimensional sp^2-carbon hexagonal lattice with one-atom thickness, has been considered as the most promising material along with PANI for supercapacitor electrodes owing to its large theoretical specific surface area of 2 675 m^2/g, high electron mobility approaching 20,000 cm^2/V s, and good mechanical properties.[25−27] For instance, in our previous study, PANI nanorods were covalently bonded on the surface of rGO, and as a result, the composite materials retained 85.3% of their initial capacitance.[20] Yu et al. prepared graphene-wrapped polyaniline nanowire arrays on a nitrogen-doped carbon fabric that retained over 94% of its initial capacitance after 5000 cycles.[23] Liu et al. demonstrated that depositing a carbonaceous shell on polyaniline and polypyrrole could greatly improve their cycle life.[24] Liu et al. have prepared a spherical tremella-like structure of a graphene−PANI composite via the self-assembly method, and the composite showed high specific capacitance and good rate performance along with a long cycle life for supercapacitors.[28] Thus, the fabricating of a desired structural material with graphene expected to enhance specific capacitance and stability is still critical.

Herein, we design and fabricate hierarchical graphene@polyaniline@graphene (G@PANI@G) sandwiches that contain hollow spheres. The general fabrication procedure is illustrated in Scheme 1. First, graphene oxide-encapsulated silica spheres ($GO@SiO_2$) were fabricated via electrostatic interactions between positively charged SiO_2 and negatively charged graphene oxide. Second, a layer of polyaniline was polymerized on the surface of $GO@SiO_2$, and then the SiO_2 was etched to form the hollow PANI@GO spheres. Lastly, G@PANI@G was obtained through a repeated self-assembly process of coating with GO and a reduction reaction. Graphene was used as both an internal skeleton shell and a cladding layer to coat the polyaniline. The hollow sandwich structure is the most important feature that is responsible for high capacitance, high rate capability, and long-term cycling stability. To optimize the electrochemical performances, the morphology of the hollow structure and the sandwich layer could be controlled through optimizing the aniline monomer concentration and the size of the SiO_2 template, respectively.

Scheme 1. Schematic Illustration of Formation Process of G@PANI@G Sandwich with Hollow Structures

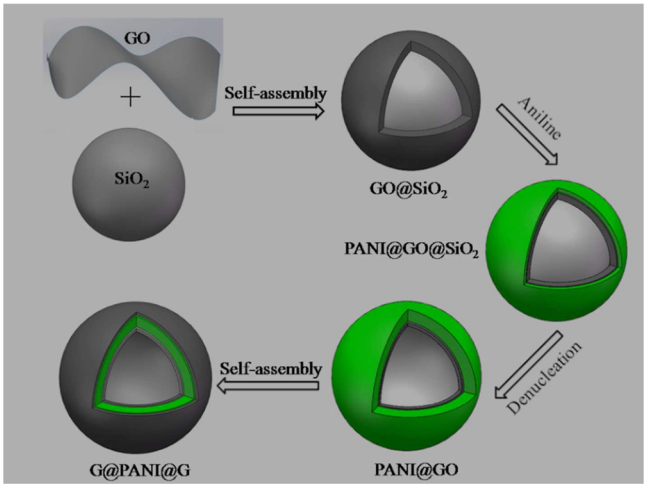

EXPERIMENTAL SECTION

Materials. Natural graphite powder (300 mesh) was purchased from the Institute of Shenghua (Changsha, China). Aminopropyltrimethoxysilane (APTMS, AR) was purchased from the Aladdin Industrial Corporation. The other reagents were purchased from Sinopharm Chemical Reagent Company (Shanghai, China). Aniline was purified by distilling it twice under a reduced pressure.

Preparation of $GO@SiO_2$. Silica spheres were obtained through the classical Stober method.[29] Then, 0.5 g of silica was dispersed in 50 mL of isopropanol via sonication, and amino-modification was reacted with 0.5 mL of APTMS under reflux for 2 h at 80 °C to synthesize APTMS−SiO_2. The graphene oxide was prepared from a natural flake graphite by an improved Hummers method.[30] A total of 500 mL of APTMS−SiO_2 solution (1 mg mL^{-1}) was gradually added to the GO solution (0.2 mg mL^{-1}) and stirred for 1 h to prepare $GO@SiO_2$. The mass ratio of APTMS−SiO_2 to GO was 5:1.

Preparation of PANI@GO. A total of 0.372 g of $GO@SiO_2$ as prepared was dispersed in 100 mL of HCl solution, and subsequently, different concentrations of aniline monomers (0.005, 0.010, and 0.020 M) were added to the solution and cooled to 4 °C. After stirring for 30 min, an ammonium persulfate (APS, 2:3 molar ratio of APS to aniline) solution was added to the mixed solution, and it was processed for 24 h. The obtained production was treated with hydrofluoric acid (HF) to remove the SiO_2.

Preparation of G@PANI@G. A 100 mL PANI@GO solution (1 mg mL^{-1}) was mixed with a 50 mL of GO solution (0.2 mg mL^{-1}) and stirred for 2 h, and last, the G@PANI@G was prepared by undergoing a reduction reaction with 0.3 mL of hydrazine at 90 °C for 2 h. The G@PANI@G with different aniline concentrations were denoted as G@PANI@G-5, G@PANI@G-10, and G@PANI@G-20. As comparison, the pure PANI was fabricated through the polymerization of aniline monomer (0.010 M) directly on the surface the APTMS−SiO_2 and denucleation of SiO_2.

Characterization. The morphologies of the samples were characterized by transmission electron microscopy (TEM, FEI Tecnai G2 F20, USA), scanning electron microscopy (SEM, ZEISS SUPRA 55, German), and atomic force microscopy (AFM, Agilent 5500, U.S.A.). The structures were investigated by X-ray diffractometry (XRD, Rigaku Ultima III, Japan), Raman spectroscopy (Renishaw Invia, U.K.), and X-ray photoelectron spectroscopy (XPS, Thermal Scientific ESCALAB 250, U.S.A.). The electrochemical measurements were carried out on an electrochemical workstation (Chenhua CHI 660D, China) based on a three-electrode system in a 1 M H_2SO_4 electrolyte solution. The working electrodes were samples of modified glassy carbon electrodes (Φ = 3 mm), and the counter electrode and reference electrode were a Pt sheet and Ag/AgCl, respectively. Typically, the obtained sample (2 mg) was dispersed in an ethanol solvent (1 mL) with Nafion solution (20 μL) to form a uniform dispersion. Then, 20 μL of mixed dispersion was dripped onto the glassy carbon electrode and dried at room temperature to obtain the working electrodes.

RESULTS AND DISCUSSION

The SiO_2 spheres prepared by the Stober method are characterized by SEM, as shown in Figure 1a. SiO_2 spheres are uniform in size with an average diameter of approximately 420 nm. After reacting with APTMS, the amino-modified SiO_2 spheres were assembled with negatively charged GO to form $GO@SiO_2$ via electrostatic interactions. The GO with a size of 3−4 μm could fully wrap round the SiO_2 spheres, which is confirmed in Figure 1b and c. Then PANI was incorporated on the $GO@SiO_2$ by polymerizing the aniline monomers to form PANI@G@SiO_2. As shown in Figure 1d, the spheres are inlayed and interconnected, indicating that PANI was

DOI: 10.1021/sc5006999
ACS Sustainable Chem. Eng. 2015, 3, 475−482

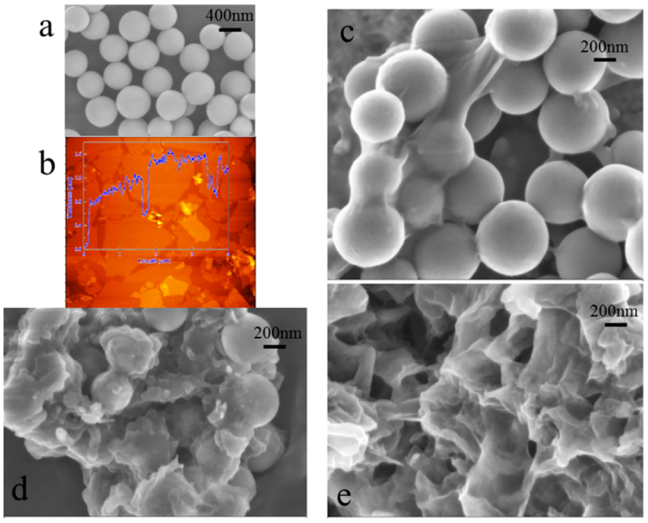

Figure 1. (a) SEM image of SiO_2, (b) AFM image of GO, and SEM images of (c) GO@SiO_2, (d) PANI@GO@SiO_2, (e) G@PANI@G.

successfully grown on the surface of GO@SiO_2. Last, from the PANI@G@SiO_2 template, the SiO_2 was etched away by HF, followed by the assembly with GO as a cladding layer and reduction of GO into reduced graphene oxide using hydrogen iodide (HI). Figure 1e shows that the structure of G@PANI@G is intact without collapse. This is because GO is first introduced onto the surface of SiO_2 as an internal skeleton shell to support the growth of PANI. Both the internal and cladding graphene layer can improve the conductivity of hybrid materials. As shown in Table 1S of the Supporting Information, the electrical conductivity of G@PANI@G (39.1 S cm^{-1}) was advanced compared with pure PANI (8.4 S cm^{-1}) and G@PANI (27.6 S cm^{-1}).

The assembly processes were further confirmed by TEM. In Figure 2a, the large scale graphene oxide sheets fully wrapped

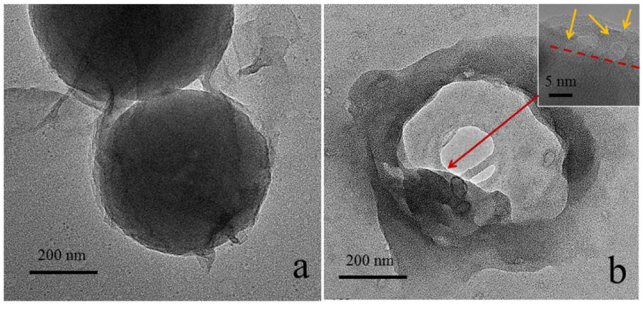

Figure 2. TEM images of (a) GO@SiO_2 and (b) G@PANI@G.

the spheres, and the edge was wrinkled and folded due to the flexibility of graphene. Meanwhile, the graphene oxide can be observed between the adjacent spheres. The feature of the G@PANI@G sandwich with hollow structures also are demonstrated in Figure 2d. In the individual particles, the hollow structure of the PANI layer is submicron and stable, which was firmed by the graphene layer with trilaminar sheets (inset enlarge TEM image). The hollow structure with graphene greatly enlarged the specific surface area. As shown in Table 1S of the Supporting Information, a high BET surface area of 241.3 m^2 g^{-1} was achieved for G@PANI@G, which was much higher than that of pure PANI and G@PANI.

XRD, Raman, and XPS were used to confirm the crystal structure and composition of the products. As shown in Figure 3a, GO shows a typical peak at $2\theta = 9.4°$, corresponding to the (001) diffraction peak. After reduction, a weak and broad peak at 24.6° was detected, demonstrating the successful preparation of rGO. For pure PANI, the two broad peaks at $2\theta = 19.8°$ and 24.9°, corresponding to the (020) and (200) crystal planes of PANI, indicated that it was an emeraldine salt.[31] In the XRD spectra of G@PANI@G, it is evident that the peaks at 9.4° and 24.6° have disappeared, and this presents peaks similar to pure PANI, which indicates that the rGO sheets were completely exfoliated and evenly covered the PANI. In the Raman spectra of GO and rGO (Figure 3b), two apparent peaks at 1350 and 1598 cm^{-1} that represent the conversion of sp^2-hybrids to sp^3-hybrids and in-plane vibrations of sp^2-hybrids, respectively, were observed. The decrease in the ratio (I_D/I_G) demonstrates GO was reduced to rGO. In particular, the intensities of the two peaks were weakened in the Raman spectrum for G@PANI@G, which was likely caused by the strong interactions between the reduced graphene oxide and PANI. Besides, the peaks at 1163, 1231, 1329, and 1488 cm^{-1} were ascribed to PANI. In addition, the peak at 2683 cm^{-1} (2D) of G@PANI@G was related to a three-layer graphene (Figure 3c), which was consistent with the TEM image.[32] The XPS survey spectrum of G@PANI@G (Figure 3d) shows the presence of oxygen (O 1s, ~532 eV), nitrogen (N 1s, ~400 eV), and carbon (C 1s, ~285 eV). In Figure 3e of the N 1s region, the N 1s peak is split into three peaks at 399.3, 399.8 ,and 400.9 eV, which are assigned to quinonoid amine (=N−), benzenoid amine (−NH−), and nitrogen cationic amine ($-N^+-$).[33,34] By calculating, the N doping content is 51.6%, demonstrating the high conductivity of G@PANI@G.

G@PANI@G with different morphology of the PANI sandwich layer can be prepared by changing the aniline monomer concentration. When the concentration is 0.005 M, the PANI layer is too thin to disconnect (Figure S1a, Supporting Information). The sandwich hollow structure showed in Figure S1b of the Supporting Information is the most uniform and stable. With the concentration increasing to 0.02 M, the PANI layer becomes nonuniform due to the polymerization of excess aniline monomers, and the hollow structure is suppressed leading to contraction (Figure S1c, Supporting Information).

The electrochemical performances of the G@PANI@G with different morphology of the sandwich PANI layer are discussed using standard cyclic voltammetry (CV), galvanostatic charge−discharge. The corresponding CV curves at 5 mV s^{-1} are shown in Figure 4a. The G@PANI@G-10 possesses the highest peak current, and the galvanostatic charge−discharge curves at 1 A g^{-1} are shown in Figure 4b. G@PANI@G-10 exhibits the longest discharge time, indicating superior electrochemical performance. The poor performance of G@PANI@G-5 is mainly caused by the disconnected PANI layer as shown in the TEM image (Figure S1a, Supporting Information). Conversely, the unevenness and contraction of the sandwich hollow structure reduces the electrode−electrolyte interface areas and increases the electrolyte ionic diffusion path leading to a decrease in the pseudocapacitance of G@PANI@G-20. Therefore, the concentration of 0.01 M is chosen for the sandwiched hollow structure with optimized electrochemical performance.

As a template, the size of the SiO_2 spheres is crucial for determining the morphology of the G@PANI@G hollow structure, which greatly influences the electrochemical perform-

DOI: 10.1021/sc5006999
ACS Sustainable Chem. Eng. 2015, 3, 475−482

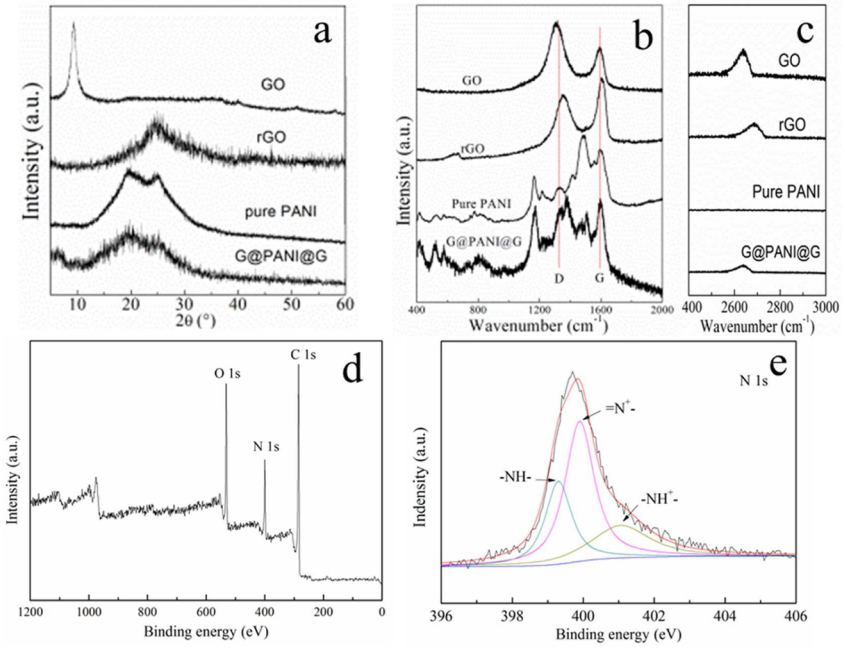

Figure 3. (a) XRD patterns and (b) Raman spectra of GO, rGO, pure PANI, and G@PANI@G. XPS spectra of G@PANI@G: (c) survey spectrum and (d) N 1s region.

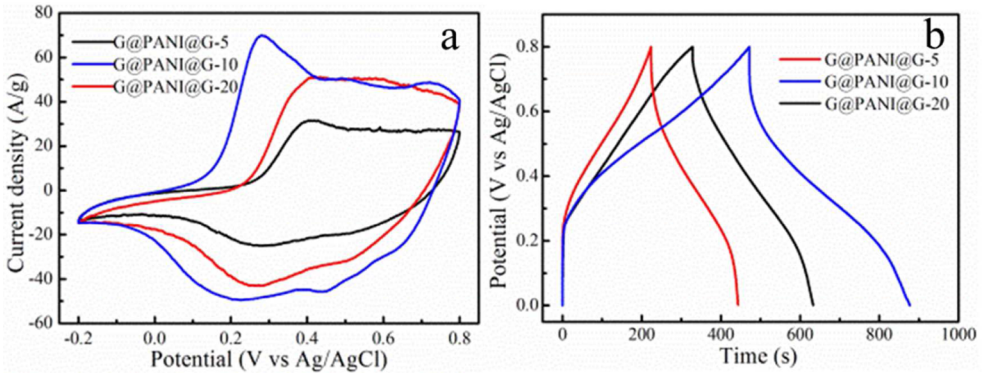

Figure 4. (a) CV curves and (b) galvanostatic charge−discharge curves of G@PANI@G with different aniline concentrations.

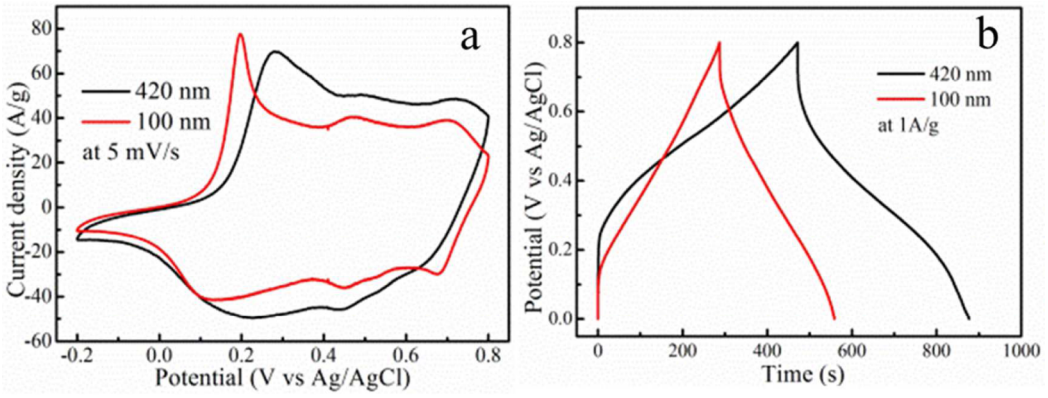

Figure 5. (a) CV curves and (b) galvanostatic charge−discharge curves of G@PANI@G from SiO_2 spheres with different sizes.

ances. Therefore, G@PANI@G hybrids prepared from two different diameters of 420 and 100 nm were used for the investigation of the electrochemical performances. The corresponding CV curves and galvanostatic charge−discharge curves are shown in Figure 5. The results show that for 420 nm G@PANI@G has the larger area of surrounding CV loop (Figure 5a) and the longer discharge time (Figure 5b), revealing that it had a superior electrochemical performance. The poor electrochemical performance is probably due to the disconnected multiholes, resulting in decreasing electroactive

DOI: 10.1021/sc5006999
ACS Sustainable Chem. Eng. 2015, 3, 475−482

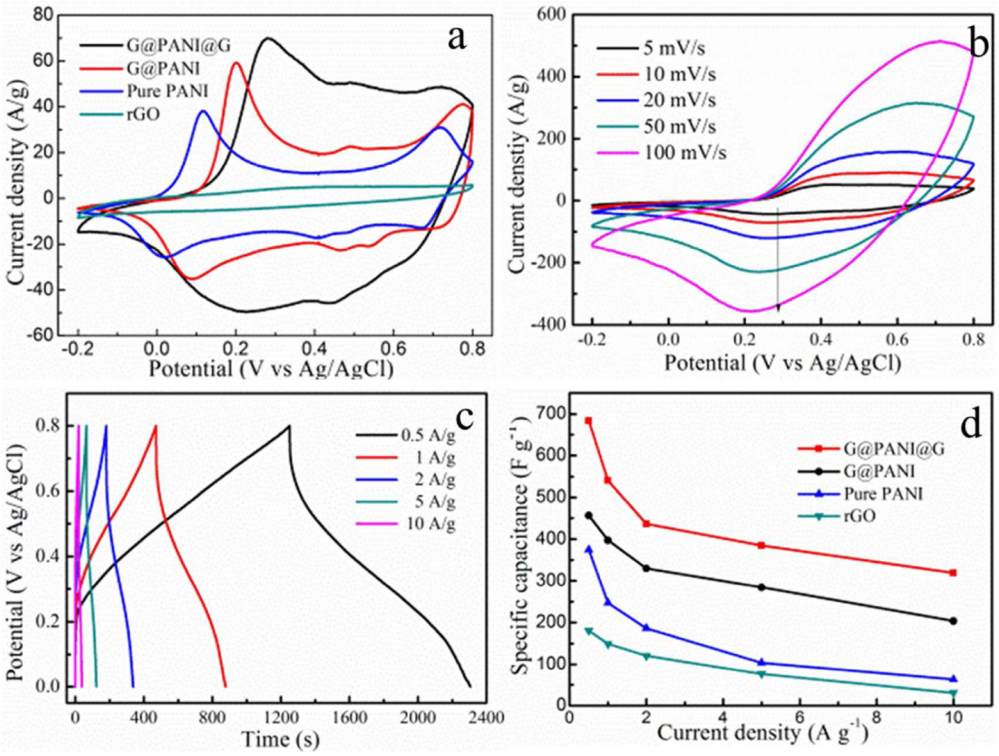

Figure 6. (a) CV curves of G@PANI@G, G@PANI, pure PANI, and rGO. (b) CV curves of G@PANI@G at different scan rates. (c) Galvanostatic charge−discharge curves of G@PANI@G at different current densities. (d) Plots of specific capacitance for G@PANI@G, G@PANI, pure PAN,I and rGO at various current densities.

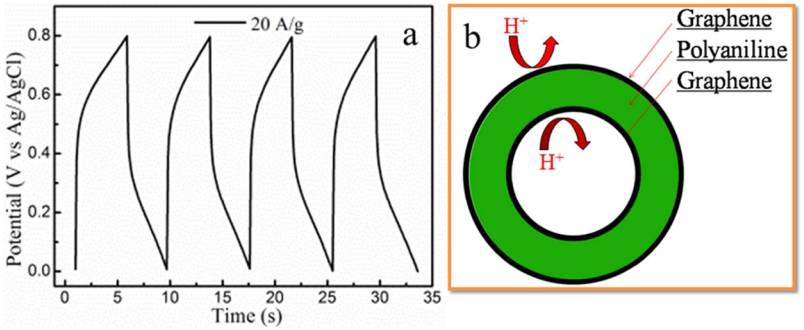

Figure 7. (a) Galvanostatic charge−discharge curve of G@PANI@G at high current density of 20 A g^{-1}. (b) Schematic illustration of the path of electrolyte ion transport at the sandwiched hollow structure.

regions, which is demonstrated by the SEM image in Figure S2 of the Supporting Information. When the size of the SiO_2 spheres is 100 nm, the PANI molecular chains are long so that the hollow structures are isolated. Therefore, G@PANI@G prepared using SiO_2 spheres with diameters of 420 nm has the optimal morphology for the electrochemical performance.

Next, G@PANI@G with superior properties prepared using the aniline monomer with a concentration of 0.010 M and SiO_2 spheres with a diameters of 420 nm was chosen for further study. Figure 6a illustrates the CVs of G@PANI@G, G@PANI, pure PANI, and rGO at a scan rate of 5 mV s^{-1}. The CV of rGO displays a nearly rectangular shape, while the CVs of G@PANI@G, G@PANI, and pure PANI present two pairs of redox peaks, which are the characteristics of pseudocapacitance. It is easily observed that the area of the surrounding CV loops of G@PANI@G is larger than the areas of the single component, which indicates a higher specific capacitance. The excellent electrochemical capability can be attributed to the unique structure. The sandwich structure provides a larger electrode−electrolyte interface area and higher conductivity. The CVs of G@PANI@G at various scan rates were investigated. As shown in Figure 6b, the peak current densities increase nearly linearly with the scan rates, indicating the rapid redox reaction of G@PANI@G. This is associated with excellent electrical conductivity. These results imply that the sandwich structure promotes the electrochemical capability of G@PANI@G.

In order to estimate the influence of the current densities on the specific capacitance of G@PANI@G specifically, the charge−discharge curves at current densities ranges of 0.5−10 A g^{-1} are shown in Figure 6c. The discharge curves show two voltage stages in the ranges of 0.8−0.45 and 0.45−0 V. The former stage with a relatively short discharge duration is due to the EDL capacitance, while the latter stage with a much longer discharge duration is associated with a combination of EDL and pseudocapacitive capacitance. At a higher current density,

DOI: 10.1021/sc5006999
ACS Sustainable Chem. Eng. 2015, 3, 475−482

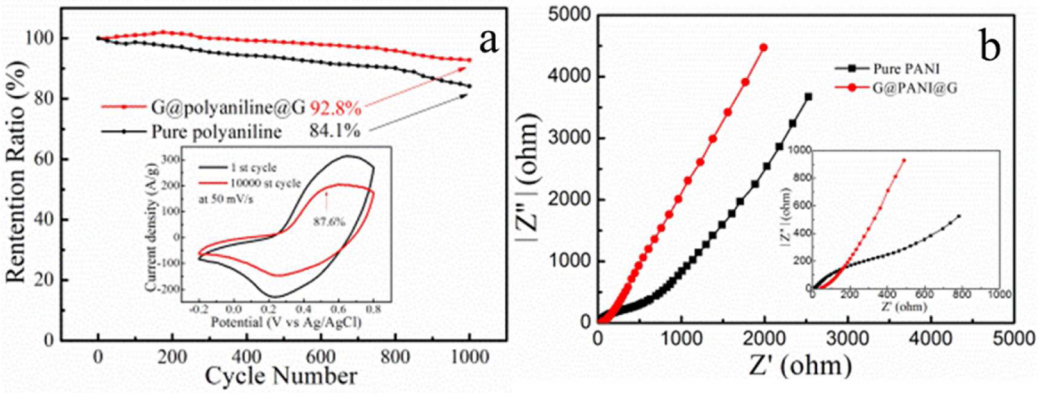

Figure 8. (a) Cycling stability and (b) Nyquist plots of G@PANI@G and pure PANI.

discharge time is lower showing that the EDL capacitance is dominant. This is possibly due to the fact that the ionic diffusion possesses time constraints that limit the electrolyte ions from accessing the pseudocapacitive materials.

The special capacitance (C_s, F/g) was calculated from the discharge stage according to the following equation:

$$C_s = \frac{I\Delta t}{\Delta V \times m}$$

where I (A), Δt (s), and ΔV (V) are the discharge current, time, and potential window in the charge−discharge curve, respectively, and m (g) is the mass of the active material. A comparison of rate capability among G@PANI@G, G@PANI, pure PANI, and rGO is shown in Figure 6d. The capacitance of G@PANI@G is 682.75 F g^{-1} at a current density of 0.5 A g^{-1}. With the current density increasing to 10 A g^{-1}, the capacitance is still 319.24 F g^{-1}. The retention rate of the specific capacitance is 46.8%, which is higher than those of G@PANI (40.3%) and pure PANI (32.7%). Further, when the current density is up to 20 A g^{-1}, the electrode of G@PANI@G still exhibits an excellent charge−discharge characteristic with a specific capacitance of 217.11 F g^{-1} (Figure 7a). This result is mainly explained by the following three factors. First, the sandwich structure greatly improves the EDL capacitance by forming a hollow structure, which could adsorb electrolyte ions in the periphery as well as in the endothecium. Second, the sandwich structure enhances the pseudocapacitance by a high utilization of PANI. Third, the wrapping with graphene layers accelerates the charge transfer and charge transport during the charge−discharge process. Thus, all of the results are in favor of a good rate capability of G@PANI@G, indicating that this is promising for application as electrode materials for supercapacitors (Figure 7b).

The cycling performance is another important factor used to determine the electrodes for practical application. The cycling tests for G@PANI@G and pure PANI are carried out at a current density of 1 A g^{-1} first. As shown in Figure 8a, G@PANI@G exhibits a better cycling stability (92.8%) than pure PANI (84.1%). Meanwhile, the performance of G@PANI@G as an electrode has been tested at a scan rate of 50 mV s^{-1} for 10,000 cycles. A total of 87.6% of the specific capacitance could be maintained, which is positive for practical application and better than that of previous reports.[20,28] During the oxidation−reduction process, pure PANI hollow spheres collapse caused by swelling or shrinking so that the specific capacitance decayed sharply. Therefore, when PANI is wrapped in graphene layers, which serves as physical buffering layers or networks to maintain the structural integrity, the stability is greatly improved.

Electrochemical impedance spectroscopy (EIS) is tested in the frequency range from 10^5 to 10^{-2} Hz with an amplitude of 20 mV. As shown in Figure 8b, both G@PANI@G and pure PANI follow Nyquist plots with an inconspicuous semicircle in the high-frequency region and a straight line in the low-frequency region. The diameter of the semicircle is related to the interfacial charge-transfer resistance (R_{st}). The R_{st} of G@PANI@G is smaller than that of pure PANI. This could be explained by the sandwich structure shortening the electrolyte ion diffusion path and facilitating the electron into the interior of the electrodes.

Furthermore, to know the applicability of the unique materials, power density and energy density, which are two important parameters for full supercapacitors, were estimated based on asymmetric supercapacitors. Figure 9 shows the

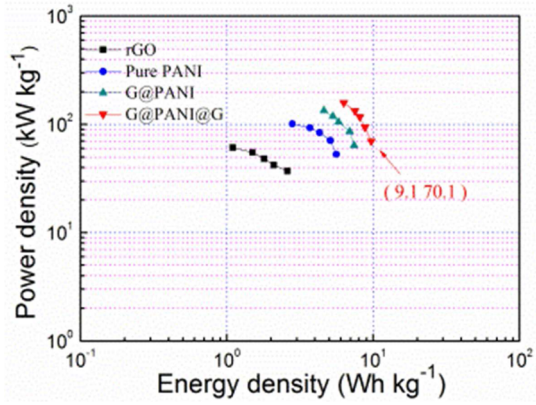

Figure 9. Range plots of energy density verse power density for rGO, pure PANI, G@PANI, and G@PANI@G at different charge−discharge current densities.

comparison of Ragone plots for rGO, pure PANI, G@PANI, and G@PANI@G. G@PANI@G exhibits the maximum energy density of 9.7 Wh kg^{-1} with a power density of 70.1 kW kg^{-1} (at 0.5 A g^{-1}), which are higher than those of the three other materials.

CONCLUSIONS

In conclusion, we have successfully demonstrated the rational design and fabrication of a graphene@polyaniline@graphene

DOI: 10.1021/sc5006999
ACS Sustainable Chem. Eng. 2015, 3, 475−482

sandwich containing hollow structures. With this unique sandwiched hollow structure, the fabricated electrode of G@PANI@G could absorb more electrolyte ions, shorten the electronic transmission path, and promote the utilization of active materials, leading to excellent electrochemical performance, which inlcudes a specific capacitance of 682.75 F g^{-1} at 0.5 A g^{-1} and good charge−discharge rate capability at high current densities. More importantly, wrapping PANI with two graphene layers as the internal skeleton shell and the cladding layer improves its stability. Therefore, the G@PANI@G has a long-term cycling stability, and the specific capacitance of 87.6% could be retained. The G@PANI@G electrodes show a maximum energy density of 9.7 Wh kg^{-1} with a power density of 70.1 kW kg^{-1}. Therefore, such designed materials could be considered as perspective electrodes for high performance supercapacitors. Furthermore, the ideation of constructing stable materials could open up a brand new field for fabricating supercapacitors.

■ ASSOCIATED CONTENT

Supporting Information

Additional information regarding characterization and results of obtained materials. This material is available free of charge via the Internet at http://pubs.acs.org.

■ AUTHOR INFORMATION

Corresponding Author

*Fax: (+86) 591 22866529. E-mail: yyzheng@fzu.edu.cn.

Notes

The authors declare no competing financial interest.

■ ACKNOWLEDGMENTS

This work was supported by the Scientific and Technological Innovation Project of Fujian Province (Grant 2012H6008) and Scientific and Technological Innovation Project of Fuzhou City (Grant 2013-G-92).

■ REFERENCES

(1) Simon, P.; Gogotsi, Y. Materials for electrochemical capacitors. *Nat. Mater.* **2008**, *7*, 845−854.

(2) Hadjipaschalis, I.; Poullikkas, A.; Efthimiou, V. Overview of current and future energy storage technologies for electric power applications. *Renewable Sustainable Energy Rev.* **2009**, *13*, 1513−1522.

(3) Zhang, J.; Lee, J. W. Supercapacitor electrodes derived from carbon dioxide. *ACS Sustainable Chem. Eng.* **2013**, *2*, 735−740.

(4) Conway, B. Electrochemical Supercapacitor. In *Scientific Fundamentals and Technological Applications*; Kluwer Academic/Plenum Publishers: New York, 1999.

(5) Zhai, Y.; Dou, Y.; Zhao, D.; Fulvio, P. F.; Mayes, R. T.; Dai, S. Carbon materials for chemical capacitive energy storage. *Adv. Mater.* **2011**, *23*, 4828−4850.

(6) Liu, X.; Wu, D.; Wang, H.; Wang, Q. Self-recovering tough gel electrolyte with adjustable supercapacitor performance. *Adv. Mater.* **2014**, *26*, 4370−4375.

(7) Chen, L. F.; Yu, Z. Y.; Ma, X.; Li, Z. Y.; Yu, S. H. In situ hydrothermal growth of ferric oxides on carbon cloth for low-cost and scalable high-energy-density supercapacitors. *Nano Energy* **2014**, *9*, 345−354.

(8) Wang, G.; Zhang, L.; Zhang, J. A review of electrode materials for electrochemical supercapacitors. *Chem. Soc. Rev.* **2012**, *41*, 797−828.

(9) Zhi, M.; Yang, F.; Meng, F.; Li, M.; Manivannan, A.; Wu, N. Effects of pore structure on performance of an activated-carbon supercapacitor electrode recycled from scrap waste tires. *ACS Sustainable Chem. Eng.* **2014**, *2*, 1592−1598.

(10) Yu, G.; Hu, L.; Liu, N.; Wang, H.; Vosgueritchian, M.; Yang, Y.; Cui, Y.; Bao, Z. Enhancing the supercapacitor performance of graphene/MnO_2 nanostructured electrodes by conductive wrapping. *Nano Lett.* **2011**, *11*, 4438−4442.

(11) Gupta, V.; Miura, N. High performance electrochemical supercapacitor from electrochemically synthesized nanostructured polyaniline. *Mater. Lett.* **2006**, *60*, 1466−1469.

(12) Wang, K.; Wu, H.; Meng, Y.; Wei, Z. Conducting polymer nanowire arrays for high performance supercapacitors. *Small.* **2014**, *10*, 14−31.

(13) Cong, H. P.; Ren, X. C.; Wang, P.; Yu, S. H. Flexible graphene−polyaniline composite paper for high-performance supercapacitor. *Energy Environ. Sci.* **2013**, *6*, 1185−1191.

(14) Xu, J.; Wang, K.; Zu, S. Z.; Han, B. H.; Wei, Z. Hierarchical nanocomposites of polyaniline nanowire arrays on graphene oxide sheets with synergistic effect for energy storage. *ACS Nano* **2010**, *4*, 5019−5026.

(15) Hu, H.; Liu, S.; Hanif, M.; Chen, S.; Hou, H. Three-dimensional cross-linked carbon network wrapped with ordered polyaniline nanowires for high-performance pseudo-supercapacitors. *J. Power Sources* **2014**, *268*, 451−458.

(16) Zhu, Z.; Wang, G.; Sun, M.; Li, X.; Li, C. Fabrication and electrochemical characterization of polyaniline nanorods modified with sulfonated carbon nanotubes for supercapacitor applications. *Electrochim. Acta* **2011**, *56*, 1366−1372.

(17) Li, Y.; Zhao, X.; Yu, P.; Zhang, Q. Oriented arrays of polyaniline nanorods grown on graphite nanosheets for an electrochemical supercapacitor. *Langmuir* **2012**, *29*, 493−500.

(18) Mi, H.; Zhang, X.; Yang, S.; Ye, X.; Luo, J. Polyaniline nanofibers as the electrode material for supercapacitors. *Mater. Chem. Phys.* **2008**, *112*, 127−131.

(19) Zhang, K.; Zhang, L. L.; Zhao, X.; Wu, J. Graphene/polyaniline nanofiber composites as supercapacitor electrodes. *Chem. Mater.* **2010**, *22*, 1392−1401.

(20) Liu, X.; Shang, P.; Zhang, Y.; Wang, X.; Fan, Z.; Wang, B.; Zheng, Y. Three-dimensional and stable polyaniline-grafted graphene hybrid materials for supercapacitor electrodes. *J. Mater. Chem. A* **2014**, *2*, 15273−15278.

(21) An, J.; Liu, J.; Zhou, Y.; Zhao, H.; Ma, Y.; Li, M.; Yu, M.; Li, S. Polyaniline-grafted graphene hybrid with amide groups and its use in supercapacitors. *J. Phys. Chem. C* **2012**, *116*, 19699−19708.

(22) Kumar, N. A.; Choi, H. J.; Shin, Y. R.; Chang, D. W.; Dai, L.; Baek, J. B. Polyaniline-grafted reduced graphene oxide for efficient electrochemical supercapacitors. *ACS Nano* **2012**, *6*, 1715−1723.

(23) Yu, P.; Li, Y.; Zhao, X.; Wu, L.; Zhang, Q. Graphene-wrapped polyaniline nanowire arrays on nitrogen-doped carbon fabric as novel flexible hybrid electrode materials for high-performance supercapacitor. *Langmuir* **2014**, *30*, 5306−5313.

(24) Liu, T.; Finn, L.; Yu, M.; Wang, H.; Zhai, T.; Lu, X.; Tong, Y.; Li, Y. Polyaniline and polypyrrole pseudocapacitor electrodes with excellent cycling stability. *Nano Lett.* **2014**, *14*, 2522−2527.

(25) Allen, M. J.; Tung, V. C.; Kaner, R. B. Honeycomb carbon: A review of graphene. *Chem. Rev.* **2009**, *110*, 132−145.

(26) Xu, C.; Xu, B.; Gu, Y.; Xiong, Z.; Sun, J.; Zhao, X. Graphene-based electrodes for electrochemical energy storage. *Energy Environ. Sci.* **2013**, *6*, 1388−1414.

(27) Stankovich, S.; Dikin, D. A.; Dommett, G. H.; Kohlhaas, K. M.; Zimney, E. J.; Stach, E. A.; Piner, R. D.; Nguyen, S. T.; Ruoff, R. S. Graphene-based composite materials. *Nature* **2006**, *442*, 282−286.

(28) Liu, H.; Zhang, W.; Song, H.; Chen, X.; Zhou, J.; Ma, Z. Tremella-like graphene/polyaniline spherical electrode material for supercapacitors. *Electrochim. Acta* **2014**, *146*, 511−517.

(29) Chen, D.; Li, L.; Tang, F.; Qi, S. Facile and scalable synthesis of tailored silica "nanorattle" structures. *Adv. Mater.* **2009**, *21*, 3804−3807.

(30) Marcano, D. C.; Kosynkin, D. V.; Berlin, J. M.; Sinitskii, A.; Sun, Z.; Slesarev, A.; Alemany, L. B.; Lu, W.; Tour, J. M. Improved synthesis of graphene oxide. *ACS Nano* **2010**, *4*, 4806−4814.

DOI: 10.1021/sc5006999
ACS Sustainable Chem. Eng. 2015, 3, 475−482

(31) Yang, Y.; Wan, M. Chiral nanotubes of polyaniline synthesized by a template-free method. *J. Mater. Chem.* **2002**, *12*, 897−901.
(32) Graf, D.; Molitor, F.; Ensslin, K.; Stampfer, C.; Jungen, A.; Hierold, C.; Wirtz, L. Spatially resolved Raman spectroscopy of single- and few-layer graphene. *Nano Lett.* **2007**, *7*, 238−242.
(33) Han, M. G.; Cho, S. K.; Oh, S. G.; Im, S. S. Preparation and characterization of polyaniline nanoparticles synthesized from DBSA micellar solution. *Synth. Met.* **2002**, *126*, 53−60.
(34) Lee, Y.; Chang, C.; Yau, S.; Fan, L.; Yang, Y.; Yang, L. O.; Itaya, K. Conformations of polyaniline molecules adsorbed on Au (111) probed by in situ STM and ex situ XPS and NEXAFS. *J. Am. Chem. Soc.* **2009**, *131*, 6468−6474.

DOI: 10.1021/sc5006999
ACS Sustainable Chem. Eng. 2015, 3, 475−482